Materials Informatics Screening of Li-Rich Layered Oxide Cathode Materials with Enhanced Characteristics Using Synthesis Data

Natalia Kireeva*[a, c] and Vladislav S. Pervov[b]

Lithium-ion batteries (LIBs) are the objects of active research and attract interest as important elements of near-term energy storage technologies. The ever-growing requirements for cathode materials of next-generation LIBs impel the need to screen the materials with high energy and power densities, cycling stability, rate capability, safety and compatibility with other battery elements. This study is focused on Li-rich layered oxide cathode materials as the materials candidates that are characterized by high energy density and large capacity and are therefore attractive as the potential solution for next-generation LIBs whereas moderate structural stability hinders their commercialization. Machine learning-assisted analysis of the collected experimental data has been performed for assessing the contribution of lattice doping, composition of compounds, the method and details of synthesis in the electrochemical characteristics. The possibility to relate parameters with the formation of a certain structure type (composite or solid solution), conceivable phase transformations and space charge layer formation are discussed. From this analysis, the features most probably amenable for electrochemical characteristics enhancement are distinguished and the focus area for further research is defined.

1. Introduction

Li-ion batteries (LIBs) are the objects of steady interest as the conceivable element of near-term energy storage technologies including electric vehicles, grid energy storage systems etc. The desired characteristics for cathode materials used in LIBs include high energy and power density, cycling stability and rate capability, material abundance, environmental safety and admissible handling properties. In this study, computer-aided screening is performed for Li-rich layered oxides (LRLO) as one of the most prominent candidates to the role of cathode materials of LIBs due to their high energy density and large capacity. However, large irreversible capacity loss during the first cycle, capacity fading and voltage degradation upon cycling due to the loss of structural stability followed by irreversible phase transitions as well as insufficient rate capability are factors hindering the consideration of LRLO as the cathode material for LIBs.

This study is aimed to unveil relationships between the composition, processing history (synthesis details), structure and electrochemical characteristics of Li-rich layered oxides using machine learning (materials informatics) approaches.

In particular, we consider several aspects such as: *(i)* contributions and prospects of lattice doping and tuning the composition of compounds, *(ii)* method of synthesis and impact of processing history (experimental conditions of synthesis, Li excess (wt.% excess during preparation of materials), the impact of precursors etc.), *(iii)* the possibility of elucidation structural type formation depending on the composition/synthesis parameters. The initial discharge capacity and coulombic efficiency as well as the capacity fade normalized to the number of cycles have been defined as the principal characteristics for compound optimization using regression methods.

The search of parameters/descriptors that relate the structure, composition, synthesis information with electrochemical characteristics has been performed. The machine learning-assisted data analysis allowed one to reveal several features related to synthesis route selection, possibility of defect formation and grain boundary effects that can severely affect the electrochemical characteristics of LRLO cathode materials.

Applying machine learning in materials science (or materials informatics) has become a popular practice for accelerating the screening of new materials.[1]

Materials informatics was applied in materials science in order to predict type of crystal structure being formed,[2–4] for post-processing analysis of characterization techniques,[5–9] for virtual screening of compounds with tailored properties,[10–27] in microstructural informatics[28–31] and for describing the processes at the interfaces[7] among other applications.

In this study, applied machine learning (ML) approaches are related to different groups of methods: chemography-based ones that assist in the visual data analysis, regression analysis that enable the quantitative assessment of the precursors-

[a] Dr. N. Kireeva
     Frumkin Institute of Physical Chemistry and Electrochemistry RAS, 31, Leninsky prospect, Moscow, 119071, Russian Federation
     Phone: +7 (916) 8257704
     Fax: +7 (495) 9554666
     E-mail: nkireeva@gmail.com
[b] Prof. V. S. Pervov
     Kurnakov Institute of General and Inorganic Chemistry RAS, 31, Leninsky prospect, Moscow, 119071, Russian Federation
[c] Dr. N. Kireeva
     Moscow Institute of Physics and Technology, 9, Institutsky per., Dolgoprudny, Moscow Region, 141701, Russian Federation

🖳 Supporting information for this article is available on the WWW under https://doi.org/10.1002/batt.201900186

composition-synthesis-structure-property relationships and models for evaluating the contribution of chosen parameters. First group of approaches performs data visualization in order to assess the relationships between the composition of compounds and the details of synthesis with certain structure type adopted by this compound since it is known that the given parameters significantly influence the structure type being formed.[32] In the studies published up to date, Li-rich layered oxide materials have been encountered in three forms: (i) a composite of trigonal and monoclinic structures, (ii) trigonal structure and (iii) monoclinic structure. Data visualization has been performed in the coordinates of the following parameters: composition, method of synthesis, Li source, Li excess, calcination and sintering temperatures and time using set of compounds with elucidated structures. It is assumed that compounds in close proximity to each other share the same structure type with high probability.

The second type is related to the modeling of the electrochemical characteristics of LRLO cathode materials (initial discharge capacity, coulombic efficiency and capacity fade) quantitatively, using regression models. Results analysis allowed to identify some features affecting tailored characteristics. These results can be discussed in connection with the grain boundary-related effects and structural stability.

2. Results and Discussion

2.1. Initial Analysis of Experimental Data

The collected data contains the LRLO structures with associated information on the initial discharge capacity under 0.1 C rate and coulombic efficiency for fixed potential ranges (2.0–4.8 V). From this data we preferentially selected those in which both initial discharge capacity and discharge capacity after cycling

were given. Thus, the data was selected from ca. fifty papers (the data is available as Supporting Information). The number of compounds varied depending on the property modeled (97, 80 and 77 compounds for initial discharge capacity, coulombic efficiency and capacity fade, respectively). A summary of the data considered and information on the descriptors and methods are given in Figure 1.

The descriptors used in this study contain (i) information on the composition of compounds, Ni–Mn ratio as individual descriptor and compositional disorder, (ii) atomic properties (ionic radii (Shannon), electronegativities (Li–Xue), work function and electron affinity) and (iii) synthesis data (method of synthesis, Li excess (weight %), decomposition temperature of Li and TM (Mn) precursors, processing time and temperature). The efforts of this study to take into account experimental/ synthesis data as descriptors values certainly cannot be considered as holistic ones since many factors have been left outside consideration (e.g. heating and cooling rates, chelating effects, pH, etc.), nevertheless a more extended description is not always possible. The given description of the synthesis cannot be considered as a way to obtain complete control on the final properties of materials, if this is possible in principle, but more of a way to support the screening of new compounds and new properties. It is worth noting that in our study we have used the data for only 0.1 C-rate and the results for other C-rates can differ due to the different kinetics of the processes.

Previous studies on Li-rich layered oxides have focused on the synthesis method,[33–35] Li excess during synthesis,[36] decomposition temperature of precursors[37] and temperature processing.[38] Presumably, using the information on the synthesis method implicitly as a certain parameter in modeling gives an insight into the possible degree of homogeneity, defect formation and structure morphology (e.g, surface area). The information on precursors can at least be considered as a parameter assessing the possibility of oxygen vacancies
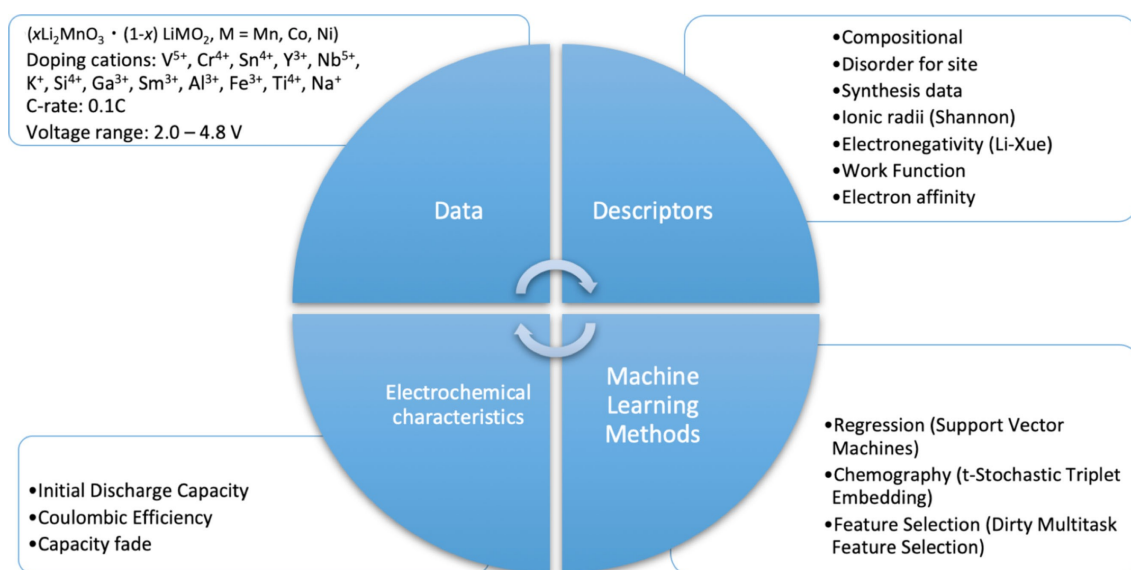

Figure 1. Considered properties, descriptor parameters, experimental data details and machine learning methods used in this study.

formation as a result of different partial oxygen pressures in the systems during synthesis. The information on Li excess introduced during synthesis was considered to affect the defect formation processes and is concerned with mitigating Ni migration[36] and possibility of multiphase product formation.[39] The Li/TM ratio has been used as descriptor for modeling as the parameter significantly affecting structural stability of compounds.[40] The method of synthesis has been encoded as descriptors' values using the experimental data of compounds with equimolar Co and Ni concentrations as a basis for introducing specific coefficients representing the relative efficiency of the synthesis approach used (introduced as coefficients 0.9, 1.0, 1.3 and 1.5 for sol-gel, co-precipitation, polymer pyrolysis and solvothermal method, respectively). Compounds synthesized with relatively rarely used synthesis methods were omitted from computations. Albeit this assumption can be seen as unreasonable it allowed us to significantly enhance the results of modeling. The descriptors describing the synthesis process are efficiently used in virtual screening applications in materials science.[41–47] Heat-treatment information including the temperature and time required for the calcination and sintering processes has been normalized to a scale of zero to one accepting the maximal and minimal known temperatures and time limits. Compositional descriptors describe the composition of compounds per formula unit (pfu). For each compound six positions in the bit string are allocated, namely - Li and Li site substituent, Mn, Ni, Co and possible dopant.

Among the composition-related descriptors one of the parameters considered in this study is the cation disorder which has been suggested in [48] and successfully applied describing the effect of ionic radii on the Curie temperature. In this study it was used for describing the atomic properties. Another one is the Ni–Mn ratio which appeared as one of the

most valuable parameters for Li-rich layered oxides. In [49] Ni–Mn interaction was supposed as a possible way of structure stabilization, the non-uniform elemental Ni–Mn distribution can provoke the phase transformation from C2/m to M_3O_4-type spinel that is absolutely undesirable since the latter one is electrochemically active only below 2 V. The composition of compounds (pfu) has been used as a multiplier in calculations of atomic properties-related descriptors in order to distinguish the compounds with different compositions.

The initial analysis of the experimental data reveals several important features. First, one can see several compounds with high initial discharge capacity characteristics (more than 240–280 mAhg^{-1}) whereas insufficient capacity retention. This behavior is observed for the compounds doped by Cr^{3+}, Fe^{3+} and Sm^{3+} cations. Among the compounds with relative structure stability one can distinguish some Co-free compounds, compounds with increased Co concentration (that can be related to the predominate formation of a trigonal LiMO2 structure) or Co-free compounds doped with cations of higher oxidation states V^{5+}, Mo^{6+}, Sn^{4+}, Nb^{5+}. For Co-free compounds one can distinguish the ones with enhanced electrochemical characteristics. It can be concerned with Mn^{3+} formation due to the presence of the oxygen vacancies in LRLO structure. Mn^{3+} participates in redox process followed by the Ni participation and, thus, at 4.8 V, the oxygen redox process presumably does not reach the stage of intensive oxygen release and, hence, the structure degradation is avoided.[50] One may note that Co substitution for the cations with higher electronegativity value (Li–Xue[51] or Martynov-Batsanov[52] scale) has a positive effect on the electrochemical characteristics of LRLO cathode materials (V^{5+}, Mo^{6+}, Sn^{4+}, Nb^{5+}).

The considered data were visualized using *t-STE* approach (Figure 2). Several observations were made. First, one can see several allocated regions on the maps. One of the regions is
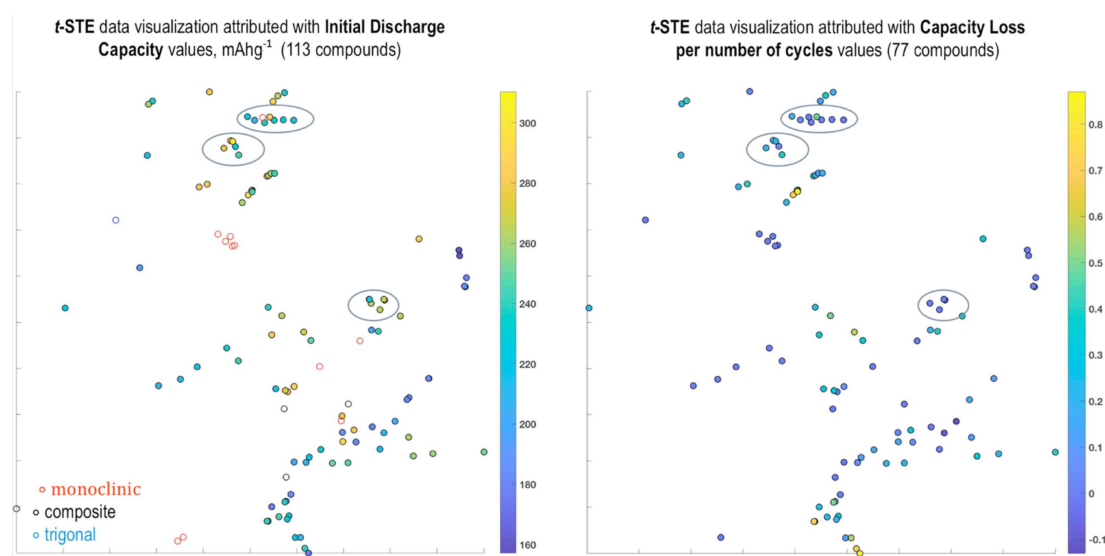

Figure 2. Analysis of the data using t-STE visualization attributed with *(a)* initial discharge capacity values, mAhg-1 and capacaty fade normalized to the number of cycles *(b)*: each point corresponds to the individual compound, the coordinates are defined by the descriptors chosen (here, composition, method of synthesis, Li source, Li excess and calcination and sintering temperature and time).

accommodated by the LRLO compounds of compositions containing Ni^{2+} and Co^{3+} in equimolar concentrations. The experimental data for these compounds is given in Figure 3. Based on the available data one can infer that a synthetic route severely affects the initial discharge capacity values. The difference in the processing conditions results in different materials morphologies and, therefore, different structural stability of the compounds due to the possible oxygen loss processes accompanied by structure degradation of the developed surfaces.[53] More dense structure forming large agglomerates can be obtained using solvothermal route (perfect electrochemical characteristics). For sol-gel synthesized compounds the opposite trend with the nucleation growth exceeding the particle growth, can be observed. And, finally, a very distinct morphology with well-developed facets for the sample obtained using the co-precipitation method can be noticed. This may be concerned with the presence of KOH in solution. One can also distinguish the compounds with both high initial discharge capacity values and minimized capacity fade (denoted in Figure).

2.2. Structure Elucidation

Several possible structures of Li-rich layered oxides are encountered in previously published studies: *(i)* intermixed nano-domains of trigonal $LiMO_2$ and monoclinic Li_2MnO_3 phases, *(ii)* single monoclinic phase, *(iii)* single trigonal phase (Figure 4). The XRD patterns of monoclinic (solid solution) and composite of monoclinic and trigonal structures are indistinguishable and due to the complexity of this structure the additional methods for structure elucidation are required. Table 1 represents the experimental data of up-to-date published studies on LRLO compounds containing the information on the method and details of synthesis, characterization technique and the LRLO structure obtained. The data on characterization techniques and possible structures are summarized in Figure 4. Table 2 represents the electrochemical characteristics for these structures if available. The mapping of the compounds with a known structure for which all the synthesis parameters were available demonstrates that almost all of the compounds with a confirmed composite structure are located in the area of equimolar Ni and Co concentrations compositions while monoclinic compounds are Co-free. The

Initial Discharge Capacity, mAhg⁻¹	Method	Precursors	Li source	Li excess	calcination temperature/ time	sintering temperature/ time
284	Co-precipitation	MnSO4·H2O, CoSO4·7H2O, NiSO4·6H2O; KOH; NH4OH; LiOH·H2O 5% excess	LiOH H20	5	450 (1h)	900 (24h)
287,5	Co-precipitation	NiSO4·6H2O, CoSO4·7H2O, MnSO4·H2O; precipitant KOH; buffering agent NH4OH; LiOH·H2O 5% excess	LiOH H20	5	450 (4h)	900 (24h)
291	Polymer-pyrolysis	LiOH·H2O, Mg(NO3)2, Ni(NO3)2·6H2O, Co-(NO3)2·6H2O, Mn(NO3)2 (50% aqueous solution) + (NH4)2S2O8	LiOH H20	0	480 (5h)	900 (12h)
296,6	Solvothermal	Mn(CH3COO)2, Ni(CH3COO)2, Co(CH3COO)2→ carbonate + 5%-excess LiOH	LiOH H20	5	500 (5h)	850 (20h)
275,9	Co-precipitation	Mn(CH3COO)2, Ni(CH3COO)2, Co(CH3COO)2→ carbonate + 5%-excess LiOH	LiOH H20	5	500 (5h)	850 (20h)
238	Sol-gel	Li(CH3COO) 2H2O, Mn(CH3COO)2 4H2O, Co(CH3COO)2 4H2O, Ni(CH3COO)2 4H2O, Cr(NO3)3 9H2O, Fe(C2O4) 2H2O, 5 % excess lithium, Citric acid	LiAc·2H2O	5	400 (12h)	875 (24h)
250	Co-precipitation	Mn(Ac)2, Ni(Ac)2, Co(Ac)2, LiOH	LiOH H20	0	480 (10h)	900 (3h)
262,5	Sol-gel	Ni(NO3)2 6H2O, Co(NO3)2 6H2O, Mn(NO3)2, LiNO3	LiNO3	0	450 (10h)	900 (3h)
241,9	Co-precipitation	MnSO4 H2O, NiSO4 6H2O, CoSO4 7H2O, Li2CO3, Na2CO3	Li2CO3	0	500 (6h)	900 (10h)
277,3	Sol-gel	(CH3COOLi 2H2O, (CH3COO)2Ni 4H2O, (CH3COO)2Co 4H2O, (CH3COO)2Mn 4H2O	LiAc·2H2O	0	400 (4h)	900 (8h)
240	Sol-gel	Li(CH3COO) 2H2O, Mn(CH3COO)2 4H2O, FeC2O4 2H2O, Ni(CH3COO)2 4H2O + 10% lithium excess, citric acid as a chelating agent	LiAc·2H2O	10	400 (3h)	850 (24h)
284,3	Sol-gel	C4H6MnO4 4H2O, C4H6NiO4 4H2O, C4H6CoO4 4H2O, C2H3O2Li 2H2O	LiAc·2H2O	0	500 (6h)	900 (12h)
260,7	Co-precipitation	MnSO4 H2O, NiSO4 6H2O, CoSO4 7H2O	LiOH H20	5	500 (5h)	900 (12h)
280,5	Glucose-assisted combustion	LiNO3, Ni(NO3)2 6H2O, Mn(NO3)2, Co(NO3)2 6H2O fuel/oxidizer=1.25	LiNO3	5	450 (3h)	900 (12h)

Co-precipitation:
Minimized calcination time and temperature (ca 450° 1-4 h)
Li source: LiOH·H2O (5% Li excess)

(a)

Calcination/Sintering: 450(1h)/900(24h)

Sol-gel:
higher temperature and longer time of calcination (ca 500° 6h)
Li source: acetates (no Li excess)

(b)

Calcination/Sintering: 500(6h)/900(12h)

Solvothermal:
higher temperature and longer time of calcination (ca 500° 5h)
Li source: hydroxide (5% Li excess)

(c)

500 nm

Calcination/Sintering: 500(5h)/850(20h)

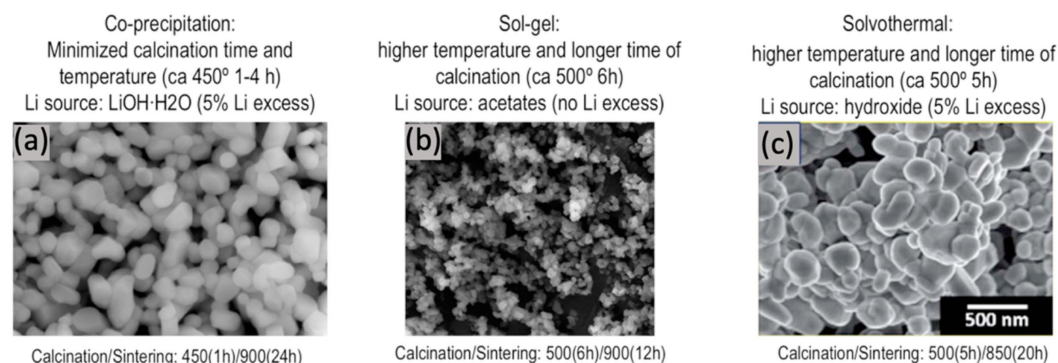**Figure 3.** Li-rich layered cathode materials compounds of $Li_{1.2}Mn_{0.54}Ni_{0.13}Co_{0.13}O_2$ composition: synthesis data and SEM data for compounds synthesized by co-precipitaion, sol-gel and solvothermal methods (SEM data reprinted with permission from [54–56]).
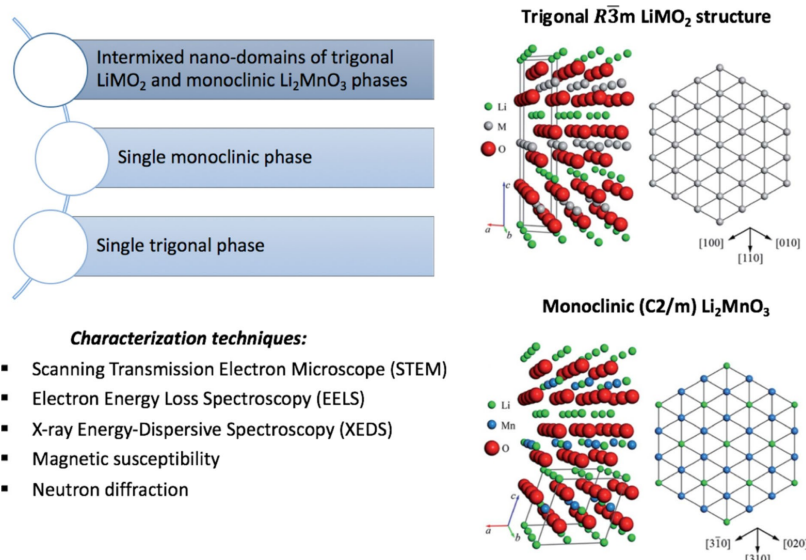
Batteries & Supercaps

Articles
doi.org/10.1002/batt.201900186

Chemistry Europe
European Chemical
Societies Publishing

Figure 4. Types of Li-rich layered oxide structures, and characterization techniques used for their structure elucidation (part of the Figure is reprinted with permission from [66]).

only compound with single trigonal phase is Co-free with Ni and Mn equimolar concentrations. The monoclinic compounds with a confirmed structure in close proximity to composites with the same composition and similar synthesis route[57] are two $Li_{1.2}Mn_{0.6}Ni_{0.2}O_{2.0}$ compounds obtained using the sol-gel method.[58,59]

In a recently published study,[32] the composition of the compounds, Li excess and cooling rate (quenching or regular cooling) were shown to be the factors severely defining the structure formation engaging the role of sintering atmosphere (oxygen), particularly. The latter detail conduces the corresponding analysis of the collected LRLO data regarding the influence and possible role of oxygen vacancies on the final LRLO structure. Another important factor is concerned with Li_2MnO_3 activation process that is highly related with compounds composition and how they are obtained. Their role in oxygen redox processes intimately associated with relaxation processes and structure reorganization affecting structure stability. By analyzing the data, we have distinguished the Co-free and Co-containing structures assuming the underlying mechanisms responsible for their electrochemical characteristics as different (in particular, we focused on compounds that are characterized by equimolar Ni and Co concentrations in one instance and Co-free compounds in another). A separate analysis of the former ones in terms of the processing temperature and precursors used (different decomposition temperature leading to different partial oxygen pressure during synthesis)[37] in connection with the experimental data analysis allows one to assume the formation of a solid solution in the case of oxygen vacancy V_o absence/depletion and liability to composite formation in a case of V_o presence. The role of oxygen vacancies in LRLO compounds seems to be of principal importance and their formation can be the function of not only the synthesis conditions but also of the interaction of different phases if the composite structure is formed. In the latter case,

one can assume high initial discharge capacity values (particularly, the larger probability of Mn^{3+} should be considered).[60] The complexity of these structures and the processes during cycling provide a means to assert them as metastable compounds. For Co-free compounds, one can assume the important role of Li excess (introduced in the process of synthesis). In [39] authors predict the multi-phase product formation as a result of Li deficiency. Another feature is concerned with the possibilities of defects-rich structure formation due to the presence of different atomic arrangements in Li_2MnO_3 structures.

2.3. Results of Modeling and Analysis of Parameters Affecting Electrochemical Characteristics

The predictive performance of the models is represented in Figure 5. The coefficient of determination (R^2) and root-mean-square error (RMSE) for the initial discharge capacity are 0.7 and 19.26, respectively, for coulombic efficiency −0.6 and 4.25 (parameters were averaged over 100 models). Despite the working character of the statistical parameters for the initial discharge capacity and coulombic efficiency the performance of the models can be considered acceptable ones and the models obtained can be used in optimization of LRLO compounds properties. For capacity fade any regression models with reasonable predictive performance were obtained. It can be explained by the difficulties in describing complex processes including structural changes and charge related effects while battery cycling.

One of the main contributions of the error that may warn their use and has to claim attention is poor property prediction for Al^{3+}, Si^{4+}, Cr^{3+}, Fe^{3+} and Ti^{4+} substituted compounds. Si substitution is characterized by its segregation (EDS elemental mapping and lattice constant values) for x = 0.04 and 0.06 Si

Table 1. Compounds with elucidated structures: their method and details of synthesis, characterization techniques have been used and confirmed structure type.

Ref.	Compound	Synthesis	Characterization technique	Structure
[61]	Li1.2Ni0.13Mn0.54Co0.13O2	Molten-salt; Li and TM nitrates; Sintering 800 °C/900 °C 8 h	HAADF-STEM, XEDS, EELS	Monoclinic (solid solution)
[62]	Li1.2Mn0.567Ni0.166Co0.067O2	SS TM acetates, LI hydroxide (5 % excess); Calcination 500 °C 5 h; Sintering 900 °C 15 h	DF-TEM, HAADF-STEM, ABF-STEM	Composite
[63]	Li1.2Mn0.55Ni0.15Co0.10O2	Unknown (purchased) Unknown (purchased)	ND + Magnetic susceptibility	Composite
[64]	Li1.2Mn0.4Co0.4O2	C—CP TM acetates, Li hydroxide; calcination 480 °C 5 h, sintering 900 ° 6 h	EXAFS	Composite
[65]	Li1.2Ni0.2Mn0.6O2, Li1.2Ni0.1Mn0.525Co0.175O2	C—CP TM sulfate hydrates, Li2CO3; calcination, sintering 900 °C 15 h	HAADF-STEM, EDS	Composite
[66]	LI1.16Mn0.625Ni0.208O2, Li1.18Mn0.612Ni0.204O2, Li1.20Mn0.6Ni0.2O2, Li1.22Mn0.588Ni0.196O2, Li1.23Mn0.577Ni0.192O2	C—CP TM sulfates, Li2CO3; calcination 500 °C 5 h; sintering 850 °C 10 h	HRTEM + SAED	Monoclinic (solid solution)
[59]	LiNi0.5Mn0.5O2, Li1.07Ni0.4Mn0.53O2, Li1.2Ni0.2Mn0.6O2	Sol-gel 900 °C (12 h), Me acetates, C—CP; 900 °C (12 h), Me hydroxides, Li excess	HAADF-STEM, D-STEM, EDS	LiNi0.5Mn0.5O2 (R m), Li1.07Ni0.4Mn0.53O2 (phase co-existence), Li1.2Ni0.2Mn0.6O2 (C2/m)
[67]	Li1.2Mn0.54Co0.13Ni0.13O2	Sol-gel, Me acetates 500 °C (5 h), sintering 800/900/1000 °C 5 h	Raman spectroscopy	Monoclinic (solid solution)
[17]	Li1.2Mn0.6Ni0.2O2	Citrate route + EDTA, Me acetates; calcination 250 °C, sintering 850 °C (5 h)	HAADF-STEM	Monoclinic (solid solution)
[49]	Li 1.2 Ni0.2Mn0.6O2	Hydrothermal, Me acetates (5 % Li excess); calcination 450 °C (12 h), sintering 900 °C (24 h)	HAADF-STEM	Monoclinic (solid solution)
[68]	Li1.2Ni0.13Co0.13Mn0.54O2	Self-combustion, Me nitrates; calcination 450 °C (2 h), sintering 700 °C (1 h), 900 °C (20 h)	NBED	Composite
[69]	Li1.2Ni0.13Co0.13Mn0.54O2	Co-precipitation, TM acetates, Li hydroxide (3 % excess); sintering 900 °C (24 h)	7Li-NMR, HAADF-STEM, EELS	Monoclinic (solid solution)
[70]	Li1.15Mn0.48Ni0.18Co0.19O2	Co-precipitation, TM sulfates, Li hydroxide; Sintering 900 °C (12 h)	SAED	Composite
[71]	Li1.2Ni0.2Mn0.6O2.0	Co-precipitation, TM sulfates, NaOH, NH3H2O; sintering 900 °C different times	HAADF-STEM	Composite
[58]	Li1.2Ni0.2Mn0.6O2.0	Sol-gel, Me acetates, EDTA, citric acid, NH4OH; calcination 450 °C (6 h); sintering 850 °C (5 h); calcination 450 °C (6 h); sintering 900 °C (24 h)	D-STEM, HAADF-STEM	Monoclinic (solid solution)
[72]	Li1.2Co0.4Mn0.4O2.0	Solid State, Li2CO3 (2 % excess), (Co0.5Mn0.5)CO3; sintering 900 °C (12 h)	HAADF-STEM, SAED	Composite
[73]	Li1.2Mn0.567Ni0.166Co0.067O2	SS, TM acetates, LIOHH20 (5 % excess); calcination 500 °C (5 h); sintering 900 °C (15 h)	HAADF-STEM, SAED	Composite
[74]	Li1.2Ni0.2Mn0.6O2.0	Co-precipitation, Ni, Mn sulfates, sodium and ammonium hydroxides, Li2CO3; sintering 900 °C (14 h)	STEM-EDS	Monoclinic
[57]	Li1.2Ni0.2Mn0.6O2.0	Co-precipitation, sol-gel, hydrothermal; SG: TM and Li acetates; calcination 450 °C (12 h); sintering 900 °C (24 h) (5 % Li excess); HA: TM and Li acetates; 450 °C (12 h)->900 °C (24 h)	HAADF-STEM	SG, CP – composite, HA – monoclinic

Batteries & Supercaps

Articles
doi.org/10.1002/batt.201900186

Chemistry Europe
European Chemical
Societies Publishing

Table 1. continued

Ref.	Compound	Synthesis	Characterization technique	Structure
[73]	Li1.2Mn0.567Ni0.166Co0.067O2	(5% Li excess) CP: TM sulfates, Li$_2$CO$_3$ 450 °C (12 h) > 900 °C (24 h) (5% Li excess) Solid-state, TM acetates, Li hydroxide (5% excess); calcination 500 °C (5 h), 900 °C (15 h)	ABF-STEM, HAADF-STEM, SAED	Composite
[75]	Li1.2Mn0.54Ni0.13 C0.13O2	Co-precipitation, TM acetates, Li hydroxide (5% excess); calcination 500 °C (5 h), sintering 900 °C (15 h)	HAADF-STEM	Monoclinic
[76]	Li1.2Mn0.54Ni0.13Co0.13O2	Molten salt: Li2CO3 (5% excess), Ni–Co–Mn oxide, 800 °C (10 h); Co-precipitation: (Ni–Co-Mn)CO$_3$ 900 °C (10 h)	TEM	Composite
[77]	Li1.2Co0.4Mn0.4O2	Solid state; sintering 900 °C (12 h)	HAADF-STEM	Composite

Table 2. Compounds with elucidated structures: initial discharge capacity values, C-rate, voltage range and confirmed structure type.

Ref.	Compound	Initial discharge capacity, mAhg^{-1}	C-rate	Voltage range, V	Structure
[64]	Li1.2Mn0.4Co0.4O2	252	0.1 C	2.5–4.8	Composite
[65]	Li1.2Ni0.2Mn0.6O2, Li1.2Ni0.1Mn0.525Co0.175O2	250	0.1 C	2.0–4.6	Composite
[66]	LI1.16Mn0.625Ni0.208O2, Li1.18Mn0.612Ni0.204O2, Li1.20Mn0.6Ni0.2O2, Li1.22Mn0.588Ni0.196O2, Li1.23Mn0.577Ni0.192O2	260 270 290 290 300	0.1 C	2.0–4.8	Monoclinic (solid solution)
[59]	LiNi0.5Mn0.5O2, Li1.07Ni0.4Mn0.53O2, Li1.2Ni0.2Mn0.6O2	190 220 235	0.25 C		LiNi0.5Mn0.5O2 (R3̄m), Li1.07Ni0.4Mn0.53O2 (phase co-existence), Li1.2Ni0.2Mn0.6O2 (C2/m)
[67]	Li1.2Mn0.54Co0.13Ni0.13O2	265	0.1 C	2.5–4.8	Monoclinic (solid solution)
[49]	Li 1.2 Ni0.2Mn0.6O2	240	0.1 C	2.0–4.8	Monoclinic (solid solution)
[68]	Li1.2Ni0.13Co0.13Mn0.54O2	284	0.1 C	2.0–4.7	Composite
[70]	Li1.15Mn0.48Ni0.18Co0.19O2	235.4/171.2 (different exposed facets)	1 C	2.0–4.8	Composite
[57]	Li1.2Ni0.2Mn0.6O2.0	SG 210CP 210HA 225	0.1 C	2.0–4.8	Monoclinic
[75]	Li1.2Mn0.54Ni0.13C0.13O2	275	0.1 C	2.0–4.8	Monoclinic
[76]	Li1.2Mn0.54Ni0.13Co0.13O2	267	0.2 C	2.0–4.8	Composite

content. The prediction of property deviates for x = 0.02 (underestimating the initial discharge capacity value) and x = 0.06 (overestimating the tailored characteristics) compounds. The reason of acceptable prediction of coulombic efficiency value here is not clear.

In the case of Al-doped sample (Li$_{1.17}$Mn$_{0.56}$Ni$_{0.2}$Co$_{0.05}$Al$_{0.02}$O$_2$) the possible explanations are not evident since the presence of at grain boundaries (GBs) is not found.

However, one can try to explain this observation (an increase in the characteristics values up to some maximum value followed by a decrease in these parameters) by means of the particle growth and the control upon surface energy of the particles. Considering one of possible explanations, the Ostwald ripening model:

$$a_t^3 - a_0^3 = \frac{8}{9}\frac{D\sigma V_m C_\infty}{RT}t$$

(where D -the diffusion coefficient, σ – surface energy, V_m – molar volume, – the equilibrium solubility, a - the particle size) one can see that at first, segregating cations can decrease surface energy of the particle thus stabilizing the structure followed by the formation of secondary possibly insulating phase that will deteriorate electrochemical characteristics.[78]

Another explanation for such a behavior is the effects related to the possibility of space charge layer formation. The model proposed in [79] can be considered as one of the possible explanations of these experimental observations. It combines the standard Poisson-Boltzmann approach with the Cahn-Hilliard model and assumes the possibility of a non-
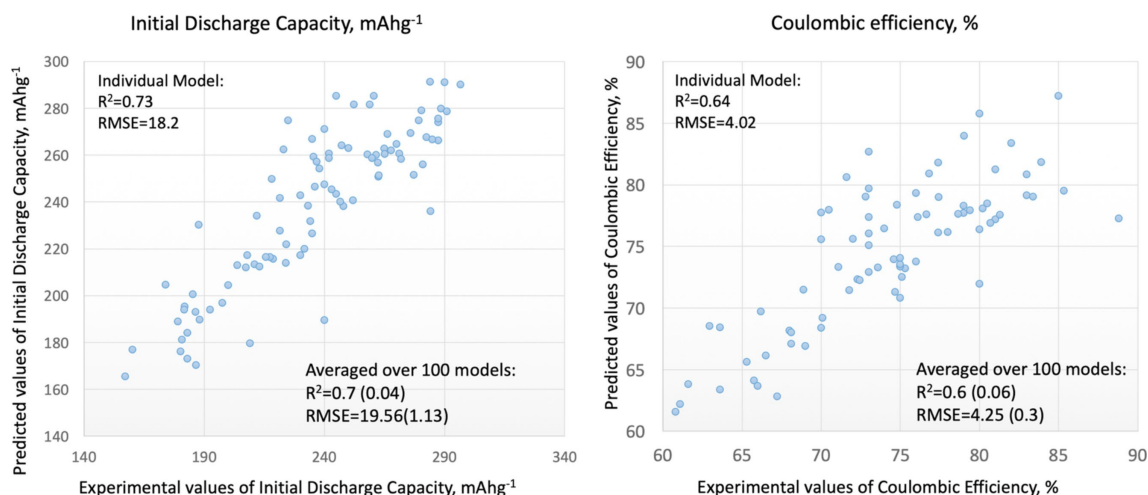
Figure 5. Results of composition-synthesis-structure-property Support Vector Machines modeling (the arbitral individual model and averaged over 100 models) of initial discharge capacity and coulombic efficiency for Li-rich layered oxides (0.1 C and 2.0–4.8 V): statistical parameters R^2 and RMSE.

monotonical increase in ionic conductivity values with a steady increase in dopant concentration due to the defects interactions resulting from the attractive interaction of dopant with oxygen vacancies, when, at some concentration threshold value, the repulsive interaction of oxygen vacancies becomes dominant.

In general, it is worth noting that the role of doped cations in relation with their grain boundary segregation can result in e.g. certain facet stabilization principally affecting the electrochemical characteristics of compounds. In the case of lithium-rich layered oxides this question has emerged in a number of studies with essential conclusions on (i) existing surfaces that are relatively stable against oxygen loss,[69,80] (ii) facet inherence to selective segregation of certain cations,[81] (iii) possibility to stabilize the high-index facets by means of cation doping, tuning the hydrolysis rate or through interactions with chelating agents,[78,82] (iv) different types of structure reconstruction depending on the developed surface[81] and (v) possible control of the particle size.[78]

For Cr^{4+} substituted sample ($x = 0.15$) a secondary phase formation (due to the migration and tetrahedral trapping of Cr ion during the redox process) is observed. This spinel phase formation is designated as a reason for the poor coulombic efficiency and capacity fade of a given sample. The authors ascribe a similar effect to Fe^{3+} substituted compounds. Accordingly, the models have the similar discrepancy between the observed and expected values both for initial discharge capacity and coulombic efficiency.

For Sn-doped LRLO oxide a secondary phase formation affecting the property value is found (SnO_2).

Unfortunately, no predictive models have been developed for capacity fade using the SVM method.

The relative contributions of the parameters chosen as descriptor values were analyzed using Dirty Feature Variable Selection method.[83] Here, the analysis of parameters contribution is two-fold. First, one can obtain a general insight on the relative influence of parameters chosen on the tailored property, initial discharge capacity in our case. Second, one can ascertain the exact difference if it is in the parameters responsible for the given property of the two considered groups of compounds for which the aforementioned difference is suspected (Co-containing and Co-free compounds). The method involved (Dirty Feature Variable Selection) is attractive due to its implicit possibility to analyze the impact of the considered parameters in relation to several properties. It comes from the assumption of a common feature space which means that analyzed parameters (descriptors) are used to solve the tasks simultaneously while distinguishing between the relevant and irrelevant parameters across the tasks. The latter one is especially important since allows one to estimate the relationships across the tasks and to identify the task-specific features. Thus, this flexible approach is used here for the analysis of relative descriptors contributions aimed at identifying the parameters distinguishing their behavior. The results of given analysis is represented in Figures 6 and 7.

From Figure 6 it can be seen that some parameters have a dominant contribution only for one compounds "class" (we consider Co-containing and Co-free compounds separately). Thus, for Co-free compounds the "favorite" (and distinct to Co-containing one) role is allocated to Mn content, decomposition temperature of Li precursor and calcination temperature, electronegativities of Ni and Mn while Co-containing compound have multiparametric dependency where one can distinguish Co content, ionic radii and electronegativity of Co, electronegativities of substituent cations, electron affinities of Ni, Co and substituent cations for TM site. Equivalent while prominent role have the calcination time, sintering temperature, decomposition temperature of Mn precursor and ionic radii disorder for site A. It should be noted that only those parameters impacting both initial discharge capacity and coulombic efficiency were considered in this analysis. Figure 7 represents the results of a similar analysis for all three properties including capacity fade. One can see the similarity from the importance of the parameters for the initial discharge capacity and coulombic efficiency. The difference in
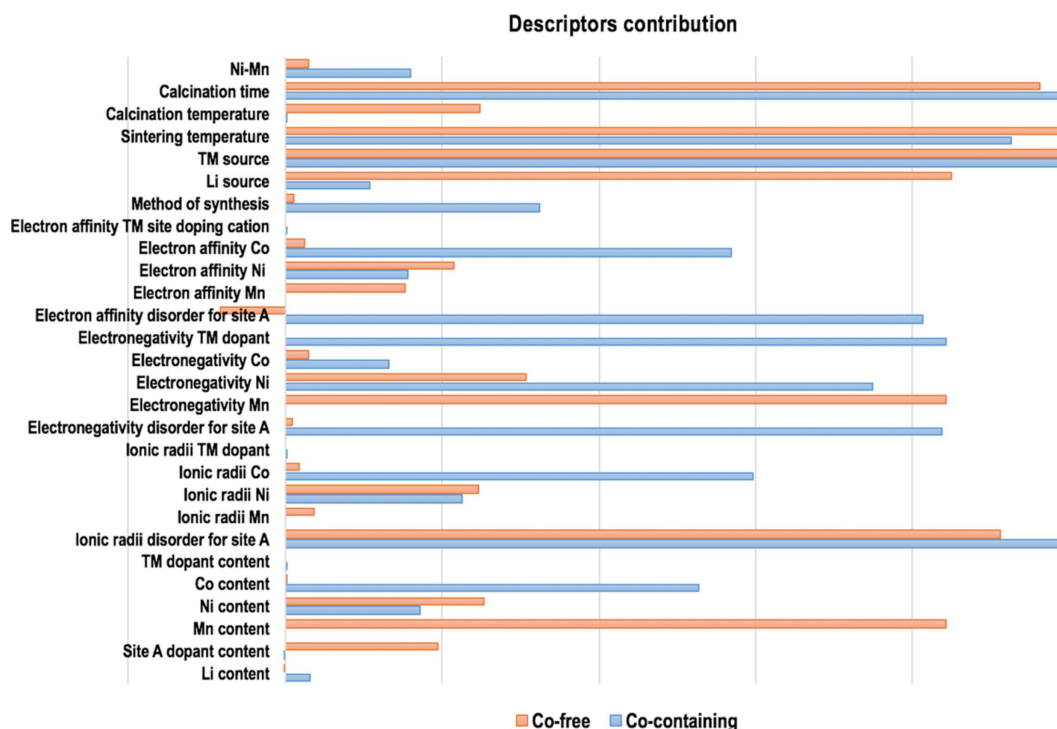
Figure 6. Relative descriptors (parameters) influence on the initial discharge capacity values for Co-free and Co-containing Li-rich layered oxide materials: parameters defining the electrochemical behavior in considered compounds groups.
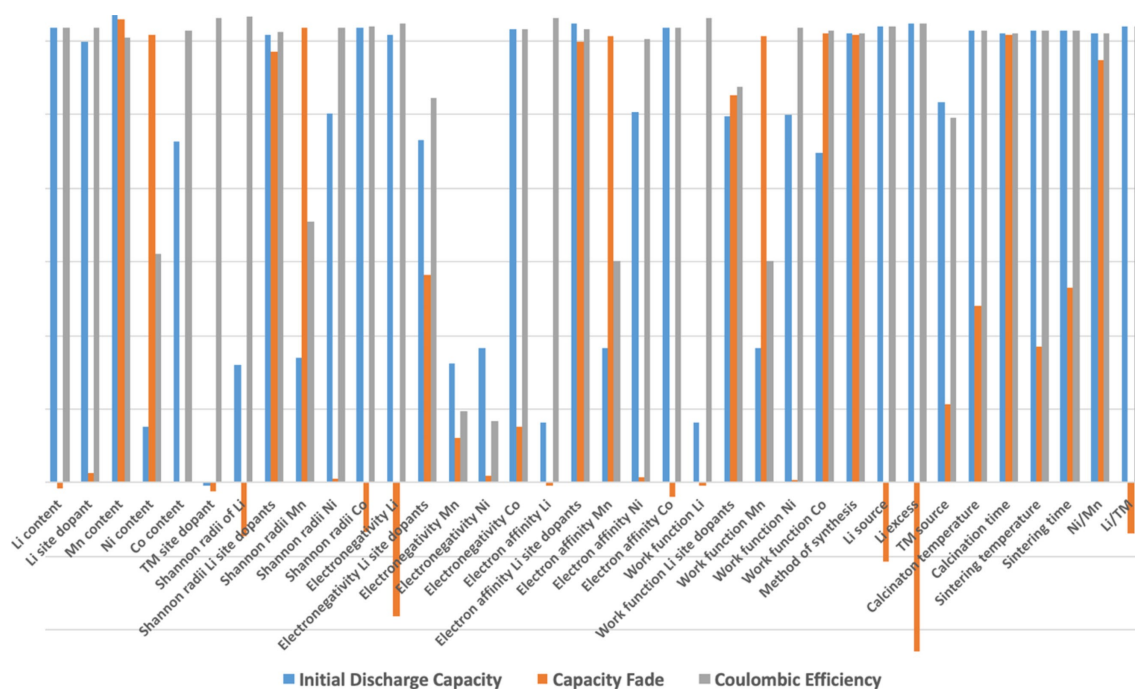

Figure 7. Relative descriptors influence on considered properties: initial discharge capacity, coulombic efficiency and capacity fade.

descriptors contribution is in the Ni content, dopants of TM site and atomic properties of Li.

The Figure also contains the information on the parameters that can be important for capacity fade. The difference in the

number of descriptors analyzed in Figures 6 and 7 are determined by different tasks.

3. Conclusions

Based on the experimental data analysis for Li-rich layered oxides followed by the modeling of their electrochemical characteristics, the parameters that are responsible for the initial discharge capacity and coulombic efficiency and can be used for property enhancement have been proposed. The results of the analysis of the parameters presumably affecting certain structure type formation for Li-rich oxides is discussed. The analysis of experimental data allows one to speculate on the role of oxygen vacancies, composition of compounds, processing temperatures and Li excess in certain Li-rich oxide structure formation. However, the precise joined impact of these parameters in combination with other ones is still not clear, and, hence, additional studies are required.

Composition-synthesis-structure property relationships for collected experimental data of the initial discharge capacity and coulombic efficiency have been assessed using Support Vector Regression. The predictive performance of the models has been assessed: the coefficient of determination (R^2) and root-mean-square error (RMSE) for initial discharge capacity are 0.7 and 19.26, for coulombic efficiency of 0.6 and 4.25 (the parameters were averaged over 100 models). Despite the moderate performance of the statistical parameters, the character of results attained allows one to bespeak the possibility to apply them for screening compounds with enhanced electrochemical characteristics. The analysis of parameters importance has been performed for considered electrochemical characteristics. The assumed difference between Co-containing and Co-free Li-rich layered oxide cathode materials in the mechanisms responsible for electrochemical characteristics has been analyzed using an approach revealing the parameters that are specifically relevant for certain Co-free or Co-containing compounds. The parameters with most valuable contribution are distinguished both for considered properties as well as for the initial discharge capacity considering Co-containing and Co-free compounds separately. Among them are processing conditions (temperature and time of calcination and sintering), Li and TM precursors, method of synthesis, Li excess, Ni–Mn ratio, Li-TM ratio, some atomic properties. Possible relations of compounds composition with cations segregation and the possibility of space charge formation is noticed as critically important for tailored electrochemical characteristics. ML approaches that have been applied in this study assisted in the analysis of multiparametric data and in the identifying parameters otherwise can be underevaluated and assessing the relative contribution of these parameters.

Experimental Section

Several machine learning approaches were utilized in this study. Machine learning-assisted experimental data visualization-based analysis has been performed with *t*-Distributed Stochastic Triplet Embedding.[84] This approach is related to dimensionality reduction methods which are also collectively known as chemography/cartography techniques in chemoinformatics. This probabilistic

approach is the efficient simulation of the concept underlying human system of judgments based on the principles of relative objects' similarity (A is more similar to B than C) which is realized in the framework of stochastic neighbor approach by maximizing the sum of the log probabilities of fairness of a given approval over all triplets of compounds in the training data:

$$\max_{x} \sum_{\forall(i,j,l)\subseteq(\tau)} \log P_{ijl} \tag{1}$$

The probabilities are defined focusing on the local similarities as follows:

$$p_{ijl} = \frac{\left(1 + \frac{\|x_i - x_j\|^2}{\alpha}\right)^{-\frac{\alpha+1}{2}}}{\left(1 + \frac{\|x_i - x_j\|^2}{\alpha}\right) - \frac{\alpha+1}{2} + \left(1 + \frac{\|x_i - x_j\|^2}{\alpha}\right)^{-\frac{\alpha+1}{2}}} \tag{2}$$

The resulting 2D map establishes the correspondence between the locations of the compounds in the chemical space defined by the coordinates adjusted during the training with compounds similarity. The number of considered triplets of compounds N = 10000.

Support Vector Machine (SVM)[85] which is a well-known supervised machine learning technique was applied to obtain a quantitative assessment of the tailored properties based on the available experimental data. In this study, LIBSVM package[86] has been used. Epsilon-SVR and Radial Basis Function (RBF) kernel functions were employed as the method's parameters. The initial data was scaled (SVM-scale package of LIBSVM). The predictive performance of each model was optimized in the grid search by varying three parameters within the given range: $C = 2^{-5}$, $2^{-3} \ldots 2^{15}$, epsilon = 0.0001, 0.001…10 (internal parameters of method) and gamma = 2^{-15}, $2^{-13} \ldots 2^3$. The models that showed the best performance on the cross-validation tuning set (part of the training) were validated on the corresponding test set. The predictive performance of the developed regression models was assessed using the ten-fold external cross-validation (10-CV) procedure where the entire dataset is divided into ten non-overlapping pairs of training and test sets of compounds. The determination coefficient R^2 and root mean squared error *RMSE* were evaluated to assess the models ability to quantitatively reproduce the experimental data.

$$R^2 = 1 - \frac{\sum_{n=1}^{N}\left(y_{pred,i} - y_{exp,i}\right)^2}{\sum_{n=1}^{N}\left(y_{exp,i} - \bar{y}_{exp,i}\right)^2} \tag{3}$$

$$RMSE = \sqrt{\frac{\sum_{n=1}^{N}}{n}\left(y_{pred,i} - y_{exp,i}\right)^2} \tag{4}$$

A third machine learning approach, Dirty Multi-Task Feature Selection,[83] was applied for descriptor analysis. This approach is based on robust prior distribution analysis and can be used to assess the individual task-focused relevance of the features as well as their importance across all the tasks considered. Using the concept of discrete mixture prior and its extensions allows one to obtain the sparse solution which is equivalent to the feature selection procedure while introducing special latent variables provides information on the specific relevance of task features or their relevance across the tasks. This is a probabilistic approach with likelihood optimization. Specifically introduced latent variables are related to five categories depending on their task and feature independence. A linear model is considered for each task:

Batteries & Supercaps

Articles
doi.org/10.1002/batt.201900186

Chemistry Europe
European Chemical
Societies Publishing

$$y^{(k)} = x^{(k)}w^{(k)} + \in^{(k)}, w^{(k)} \in \mathbb{R}^d \qquad (5)$$

The likelihood function is estimated for weights coefficients and variance of Gaussian noise:

$$p = (Y|X, W, \sigma^2) = \prod_{k=1}^{K} N(y^{(k)}|X^{(k)}w^{(k)}, I\sigma_k^2) \qquad (6)$$

The prior distribution of weights contains information on these categories:

$$p = (W|\Omega) = \prod_{i=1}^{d} \prod_{k=1}^{K} p\left(w_i^{(k)}\middle|\Omega\right) \qquad (7)$$

where Ω includes all five categories as binary latent variables:

z_i – indicates whether the feature is outlier (if it is an outlier, it can be independently considered for each task);

ω_k – indicates whether task k is an outlier task (it can contain specific relevant and irrelevant features);

γ_i – indicates whether the non-outlier feature is relevant for all tasks that are not outliers;

$\tau_i^{(k)}$ – indicates whether the feature is relevant for outlier task k;

$\eta_i^{(k)}$ – indicates whether the outlier feature is relevant.

The corresponding joint probability distribution is normalized with respect to latent variables, weight coefficients and noise.

$$p = (Y|X, W, \sigma^2) = \prod_{k=1}^{K} N(y^{(k)}|x^{(k)}w^{(k)}, I\sigma_k^2) \qquad (8)$$

Acknowledgement

[1] D. P. Tabor, L. M. Roch, S. K. Saikin, C. Kreisbeck, D. Sheberla, J. H. Montoya, S. Dwaraknath, M. Aykol, C. Ortiz, H. Tribukait, C. Amador-Bedolla, C. J. Brabec, B. Maruyama, K. A. Persson, A. Aspuru-Guzik, *Nat. Rev. Mater.* **2018**, *3*, 5–20.
[2] C. C. Fischer, K. J. Tibbetts, D. Morgan, G. Ceder, *Nat. Mater.* **2006**, *5*, 641.
[3] A. O. Oliynyk, L. A. Adutwum, B. W. Rudyk, H. Pisavadia, S. Lotfi, V. Hlukhyy, J. J. Harynuk, A. Mar, J. Brgoch, *J. Am. Chem. Soc.* **2017**, *139*, 17870–17881.
[4] W. F. Reinhart, A. W. Long, M. P. Howard, A. L. Ferguson, A. Z. Panagiotopoulos, *Soft Matter* **2017**, *13*, 4733–4745.
[5] R. K. Vasudevan, M. Ziatdinov, S. Jesse, S. V. Kalinin, *Nano Lett.* **2016**, *16*, 5574–5581.
[6] F. Vurpillot, W. Lefebvre, J. M. Cairney, C. Oberdorfer, B. P. Geiser, K. Rajan, *MRS Bull.* **2016**, *41*, 46–52.
[7] E. Strelcov, A. Belianinov, Y.-H. Hsieh, S. Jesse, A. P. Baddorf, Y.-H. Chu, S. V. Kalinin, *ACS Nano* **2014**, *8*, 6449–6457.
[8] S. V. Kalinin, B. G. Sumpter, R. K. Archibald, *Nat. Mater.* **2015**, *14*, 973.
[9] A. Belianinov, Q. He, M. Kravchenko, S. Jesse, A. Borisevich, S. V. Kalinin, *Nat. Commun.* **2015**, *6*, 7801.
[10] U. Zavyalova, M. Holena, R. Schlögl, M. Baerns, *ChemCatChem* **2011**, *3*, 1935–1947.
[11] D. A. Winkler, *Toxicol. Appl. Pharmacol.* **2016**, *299*, 96–100.
[12] Z. W. Ulissi, M. T. Tang, J. Xiao, X. Liu, D. A. Torelli, M. Karamad, K. Cummins, C. Hahn, N. S. Lewis, T. F. Jaramillo, K. Chan, J. K. Nørskov, *ACS Catal.* **2017**, *7*, 6600–6608.
[13] E. O. Pyzer-Knapp, K. Li, A. Aspuru-Guzik, *Adv. Funct. Mater.* **2015**, *25*, 6495–6502.
[14] E. O. Pyzer-Knapp, G. N. Simm, A. A. Aspuru Guzik, *Mater. Horiz.* **2016**, *3*, 226–233.
[15] F. Legrain, J. Carrete, A. van Roekeghem, S. Curtarolo, N. Mingo, *Chem. Mater.* **2017**, *29*, 6220–6227.
[16] R. Jinnouchi, R. Asahi, *J. Phys. Chem. Lett.* **2017**, *8*, 4279–4283.
[17] R. Jalem, T. Aoyama, M. Nakayama, M. Nogami, *Chem. Mater.* **2012**, *24*, 1357–1364.
[18] R. Jalem, M. Nakayama, T. Kasuga, *J. Mater. Chem. A* **2014**, *2*, 720–734.
[19] R. Jalem, M. Kimura, M. Nakayama, T. Kasuga, *J. Chem. Inf. Model.* **2015**, *55*, 1158–1168.
[20] O. Isayev, D. Fourches, E. N. Muratov, C. Oses, K. Rasch, A. Tropsha, S. Curtarolo, *Chem. Mater.* **2015**, *27*, 735–743.
[21] F. Hase, S. Valleau, E. Pyzer-Knapp, A. Aspuru-Guzik, *Chem. Sci.* **2016**, *7*, 5139–5147.
[22] R. Gomez-Bombarelli, *Nat. Mater.* **2016**, *15*, 1120–1127.
[23] V. C. Epa, A. L. Hook, C. Chang, J. Yang, R. Langer, D. G. Anderson, P. Williams, M. C. Davies, M. R. Alexander, D. A. Winkler, *Adv. Funct. Mater.* **2013**, *24*, 2085–2093.
[24] P. Dey, J. Bible, S. Datta, S. Broderick, J. Jasinski, M. Sunkara, M. Menon, K. Rajan, *Comput. Mater. Sci.* **2014**, *83*, 185–195.
[25] M. de Jong, W. Chen, R. Notestine, K. Persson, G. Ceder, A. Jain, M. Asta, A. A. Gamst, *Sci. Rep.* **2016**, *6*, 34256.
[26] P. V. Balachandran, J. Theiler, J. M. Rondinelli, T. Lookman, *Sci. Rep.* **2016**, *5*, 13285.
[27] L. Ward, A. Agrawal, A. Choudhary, C. Wolverton, *NPJ Comput. Mater.* **2016**, *2*, 16028 EP.
[28] Q. Zhu, A. Samanta, B. Li, R. E. Rudd, T. Frolov, *Nat. Commun.* **2018**, *9*, 467.
[29] H. Xu, R. Liu, A. Choudhary, W. A. Chen, *J. Mech. Des.* **2015**, *137*, 051403–051403.
[30] O. Wodo, S. Broderick, K. Rajan, *MRS Bull.* **2016**, *41*, 603–609.
[31] C. W. Rosenbrock, E. R. Homer, G. Csányi, G. L. W. Hart, *NPJ Comput. Mater.* **2017**, *3*, 29.
[32] E. McCalla, J. Li, A. W. Rowe, J. R. Dahn, *J. Electrochem. Soc.* **2014**, *161*, A606–A613.
[33] F. Fu, Q. Wang, Y.-P. Deng, C.-H. Shen, X.-X. Peng, L. Huang, S.-G. Sun, *J. Mater. Chem. A* **2015**, *3*, 5197–5203.
[34] M. G. Verde, H. Liu, K. J. Carroll, L. Baggetto, G. M. Veith, Y. S. Meng, *ACS Appl. Mater. Interfaces* **2014**, *6*, 18868–18877, PMID: 25275709.
[35] N. Yabuuchi, K. Kubota, Y. Aoki, S. Komaba, *J. Phys. Chem. C* **2016**, *120*, 875–885.
[36] W. Liu, G. Fang, B. Xia, H. Sun, S. Kaneko, D. Li, *RSC Adv.* **2013**, *3*, 15630–15635.
[37] X. Zhang, D. Luo, G. Li, J. Zheng, C. Yu, X. Guan, C. Fu, X. Huang, L. Li, *J. Mater. Chem. A* **2013**, *1*, 9721–9729.
[38] J.-M. Lim, D. Kim, Y.-G. Lim, M.-S. Park, Y.-J. Kim, M. Cho, K. Cho, *ChemElectroChem* **2016**, *3*, 943–949.
[39] Y. Pei, Q. Chen, Y.-C. Xiao, L. Liu, C.-Y. Xu, L. Zhen, G. Henkelman, G. Cao, *Nano Energy* **2017**, *40*, 566–575.
[40] R. Shunmugasundaram, R. Senthil Arumugam, J. R. Dahn, *Chem. Mater.* **2015**, *27*, 757–767.
[41] E. Kim, K. Huang, S. Jegelka, E. Olivetti, *npj Comput. Mater.* **2017**, *3*, 53.
[42] P. Raccuglia, K. C. Elbert, P. D. F. Adler, C. Falk, M. B. Wenny, A. Mollo, M. Zeller, S. A. Friedler, J. Schrier, A. J. Norquist, *Nature* **2016**, *533*, 73 .
[43] C. Klanner, D. Farrusseng, L. Baumes, C. Mirodatos, F. Schuth, *QSAR Comb. Sci.* **2003**, *22*, 729.
[44] S. R. Young, A. Maksov, M. Ziatdinov, Y. Cao, M. Burch, J. Balachandran, L. Li, S. Somnath, R. M. Patton, S. V. Kalinin, R. K. Vasudevan, *J. Appl. Phys.* **2018**, *123*, 115303.
[45] R. P. Cunha, T. Lombardo, E. N. Primo, A. A. Franco, *Batteries & Supercaps* **2020**, *3*, 60; Supercaps **2020**, 3, 60.
[46] N. Kireeva, V. S. Pervov, *PCCP* **2017**, *19*, 20904–20918.
[47] E. Kim, K. Huang, A. Saunders, A. McCallum, G. Ceder, E. Olivetti, *Chem. Mater.* **2017**, *29*, 9436–9444.
[48] A. Berenov, F. Le Goupil, N. Alford, *Sci. Rep.* **2016**, *6*, 28055.
[49] J. Zheng, P. Xu, M. Gu, J. Xiao, N. D. Browning, P. Yan, C. Wang, J.-G. Zhang, *Chem. Mater.* **2015**, *27*, 1381–1390.
[50] M. Tang, A. Dalzini, X. Li, X. Feng, P.-H. Chien, L. Song, Y.-Y. Hu, *J. Phys. Chem. Lett.* **2017**, *8*, 4009–4016.
[51] K. Li, D. Xue, *Phys. Chem. A* **2006**, *110*, 11332–11337.

[52] S. S. Batsanov, *Russ. Chem. Rev.* **1982**, *51*, 684.

[53] S. Kuppan, A. K. Shukla, D. Membreno, D. Nordlund, G. Chen, *Adv. Energy Mater.* **2017**, *7*, 1602010.

[54] T. Yu, J. Li, G. Xu, J. Li, F. Ding, F. Kang, *Solid State Ionics* **2017**, *301*, 64–71.

[55] F. Wu, H. Wang, Y. Bai, Y. Li, C. Wu, G. Chen, L. Liu, Q. Ni, X. Wang, J. Zhou, *Solid State Ionics* **2017**, *300*, 149–156.

[56] D. Dai, B. Wang, B. Li, F. Li, X. Wang, H. Tang, Z. Chang, *RSC Adv.* **2016**, *6*, 96714.

[57] J. Zheng, M. Gu, A. Genc, J. Xiao, P. Xu, X. Chen, Z. Zhu, W. Zhao, L. Pullan, C. Wang, J.-G. Zhang, *Nano Lett.* **2014**, *14*, 2628–2635, PMID: 24707978.

[58] K. Jarvis, C.-C. Wang, M. Varela, R. R. Unocic, A. Manthiram, P. J. Ferreira, *Chem. Mater.* **2017**, *29*, 7668–7674.

[59] K. A. Jarvis, C.-C. Wang, A. Manthiram, P. J. Ferreira, *J. Mater. Chem. A* **2014**, *2*, 1353–1362.

[60] S. Mandal, R. E. Cohen, K. Haule, *Phys. Rev. B* **2018**, *98*, 075155.

[61] A. K. Shukla, Q. M. Ramasse, C. Ophus, H. Duncan, F. Hage, G. Chen, *Nat. Commun.* **2015**, *6*, 8711.

[62] H. Yu, Y.-G. So, A. Kuwabara, E. Tochigi, N. Shibata, T. Kudo, H. Zhou, Y. Ikuhara, *Nano Lett.* **2016**, *16*, 2907–2915.

[63] D. Mohanty, A. Huq, E. A. Payzant, A. S. Sefat, J. Li, D. P. Abraham, D. L. Wood, C. Daniel, *Chem. Mater.* **2013**, *25*, 4064–4070.

[64] J. Rana, R. Kloepsch, J. Li, T. Scherb, G. Schumacher, M. Winter, J. Banhart, *J. Mater. Chem. A* **2014**, *2*, 9099–9110.

[65] M. Gu, I. Belharouak, J. Zheng, H. Wu, J. Xiao, A. Genc, K. Amine, S. The-vuthasan, D. R. Baer, J.-G. Zhang, N. D. Browning, J. Liu, C. Wang, *ACS Nano* **2013**, *7*, 760–767.

[66] Y. Song, X. Zhao, C. Wang, H. Bi, J. Zhang, S. Li, M. Wang, R. Che, *J. Mater. Chem. A* **2017**, *5*, 11214–11223.

[67] H. Koga, L. Croguennec, P. Mannessiez, M. Ménétrier, F. Weill, L. Bourgeois, M. Dut- tine, E. Suard, C. Delmas, *J. Phys. Chem. C* **2012**, *116*, 13497–13506.

[68] P. Kumar Nayak, J. Grinblat, E. Levi, T. R. Penki, M. Levi, Y–K. Sun, B. Markovsky, D. Aurbach, *ACS Appl. Mater. Interfaces* **2017**, *9*, 4309–4319.

[69] H. Liu, K. J. Harris, M. Jiang, Y. Wu, G. R. Goward, G. A. Botton, *ACS Nano* **2018**, *12*, 2708–2718, PMID: 29505239.

[70] D. Luo, P. shi, S. Fang, L. Yang, S. Ichi Hirano, *J. Power Sources* **2017**, *364*, 121–129.

[71] M. Gu, I. Belharouak, A. Genc, Z. Wang, D. Wang, K. Amine, F. Gao, G. Zhou, S. Thevuthasan, D. R. Baer, J.-G. Zhang, N. D. Browning, J. Liu, C. Wang, *Nano Lett.* **2012**, *12*, 5186–5191.

[72] J. Wen, J. Bareño, C. Lei, S. Kang, M. Balasubramanian, I. Petrov, D. Abraham, *Solid State Ionics* **2011**, *182*, 98–107.

[73] H. Yu, R. Ishikawa, Y.-G. So, N. Shibata, T. Kudo, H. Zhou, Y. Ikuhara, *Angew. Chem.* **2013**, *125*, 6085–6089.

[74] P. Lu, R. L. Yuan, J. F. Ihlefeld, E. D. Spoerke, W. Pan, J. M. Zuo, *Nano Lett.* **2016**, *16*, 2728–2733.

[75] X. Li, K. Zhang, D. Mitlin, Z. Yang, M. Wang, Y. Tang, F. Jiang, Y. Du, J. Zheng, *Chem. Mater.* **2018**, *30*, 2566–2573.

[76] L. Riekehr, J. Liu, B. Schwarz, F. Sigel, I. Kerkamm, Y. Xia, H. Ehrenberg, *J. Power Sources* **2016**, *325*, 391–403.

[77] J. Bareño, M. Balasubramanian, S. H. Kang, J. G. Wen, C. H. Lei, S. V. Pol, I. Petrov, D. P. Abraham, *Chem. Mater.* **2011**, *23*, 2039–2050.

[78] R. H. R. Castro, D. Gouvêa, *J. Am. Ceram. Soc.* **2016**, *99*, 1105–1121.

[79] D. S. Mebane, R. A. De Souza, *Energy Environmental Science* **2015**, *8*, 2935.

[80] Y. Shin, K. A. Persson, *ACS Appl. Mater. Interfaces* **2016**, *8*, 25595–25602, PMID: 27598948.

[81] P. Yan, J. Zheng, J. Zheng, Z. Wang, G. Teng, S. Kuppan, J. Xiao, G. Chen, F. Pan, J.-G. Zhang, C.-M. Wang, *Adv. Energy Mater.* **2016**, *6*, 1502455.

[82] A. Danks, S. Hall, Z. Schnepp, *Mater. Horiz.* **2016**, *3*, 91.

[83] D. A. Hernandez-Lobato, *Proceedings of International Conference on Machine Learning* **2015**, 1073–1082.

[84] L. Maaten, *Proceedings of the IEEE International Workshop on Machine Learning for Signal Processing* **2012**.

[85] V. N. Vapnik, *The Nature of Statistical Learning Theory* ; null; 2000; p. null.

[86] C.-C. Chang, C.-J. Lin, LIBSVM : a library for support vector machines. LIBSVM : a library for support vector machines **2001**, Software available at *http://www.csie.ntu.edu.tw/* cjlin/libsvm.